

Automatic nodule identification and differentiation in ultrasound videos to facilitate per-nodule examination

Siyuan Jiang^{a,g,1}, Yan Ding^{d,1}, Yuling Wang^{c,1}, Lei Xu^a, Wenli Dai^b,
Wanru Chang^b, Jianfeng Zhang^f, Jie Yu^c, Jianqiao Zhou^e, Chunquan
Zhang^{d,*}, Ping Liang^{c,*}, Dexing Kong^{b,*}

^aZhejiang Qiushi Institute for Mathematical Medicine, Hangzhou, 311121, China

^bSchool of Mathematical Sciences, Zhejiang University, Hangzhou, 310027, China

^cDepartment of Interventional Ultrasound, The Fifth Medical Center of Chinese PLA General Hospital, Beijing, 100853, China

^dDepartment of Ultrasound, the Second Affiliated Hospital of Nanchang University, Nanchang, 330006, China

^eDepartment of Ultrasound, Ruijin Hospital, Shanghai Jiaotong University School of Medicine, Shanghai, 200025, China

^fCollege of Mathematical Medicine, Zhejiang Normal University, Jinhua, 321004, China

^gZhejiang Demetics Medical Technology Co.,Ltd, Hangzhou, 311121, China

*Corresponding author

¹Siyuan Jiang, Yan Ding, and Yuling Wang contributed equally to this work.

Abstract

Background: Ultrasound is a vital diagnostic technique in health screening, with the advantages of being non-invasive, cost-effective, and radiation-free and therefore is widely applied in the diagnosis of nodules. However, it relies heavily on the expertise and clinical experience of the sonographer. In ultrasound images, a single nodule might present heterogeneous appearances in different cross-sectional views making it hard to perform per-nodule examination. Sonographers usually discriminate different nodules by examining the nodule features and the surrounding structures like glands and ducts, which is cumbersome and time-consuming.

Purpose: To facilitate per-nodule examination, this study develops a deep learning-based nodule differentiation system, which can identify and cluster different ultrasonic video clips by nodules in real time.

Methods: The nodule re-identification system consists of two parts: an extractor based on the deep learning model that can extract feature vector from the input video clip and a real-time clustering algorithm that automatically groups feature vectors by nodules. The extractor was trained jointly with a classification head using cross-entropy loss and contrastive loss by identifying individual nodule clips. In this process, the extractor learns a representation vector based on which the classification head assigned probability scores. In the test phase, representation vectors from different video clips are compared with cosine similarity. Video clips that have close representations

are clustered to the same nodule. To reduce clustering error, we proposed a simple but effective algorithm that outperforms common clustering algorithms both in accuracy and efficiency. We collect 3409 video clips from 787 patients to train and validate our model. The dataset was randomly divided into training(623 patients), validation(76 patients), and test(88 patients) sets. W Delong test is conducted to evaluate the statistical differences between the two models.

Results: In terms of re-identification accuracy, the experimental results suggest that the classification model outperforms the verification model, reaching AUC values of 0.9324(95% CI: 0.9110-0.9539) and 0.9087(95% CI: 0.8933-0.9242) on the validation and test set, respectively. For clustering, compared with several commonly used clustering algorithms, our algorithm obtains the best F-score of 88.26 in the least time(< 0.001s).

Conclusions: We proposed a deep learning-based system to differentiate and cluster ultrasonic video clips by nodules. While easy to implement, quantitative results show that the proposed method is accurate and efficient.

Contents

I. INTRODUCTION	1
II. METHODS	4
II.A. model structure	6
II.B. loss function	7
II.C. clustering	8
II.D. Dataset	9
II.E. Implementation details	10
III. RESULTS	11
IV. DISCUSSION	14
V. CONCLUSION	16
References	17

I. INTRODUCTION

Ultrasound examination has low risk with no ionizing radiation, and it is widely accessible with lower cost, and thus is used as the first-line screening medical imaging modality for thyroid¹, breast², liver tumors³, etc. However, as a non-standardized technology, the lesion representativeness of its acquired images is limited by the two-dimensional slices taken from the original three-dimensional volume and thus is highly dependent on its operators⁴. At present, the ultrasound evaluation of nodules requires repeated scanning to confirm the number and feature of nodules and requires scanning a single nodule from multiple sections, which makes it time-consuming and labor-intensive, sometimes difficult, to find the same nodule from multiple scanning videos of one patient especially when the states of individual nodules need to be periodically monitored during follow-up examinations⁵.

With the development of artificial intelligence, Computer-Aided Diagnosis (CAD) systems have been widely used in the medical imaging field. Recent advances in deep neural networks have improved image analysis performance⁶. The main advantage of using deep neural networks is that they can learn and extract complex patterns from raw data in a very effective way without any previous feature engineering. Most research of artificial intelligence(AI) in the field of medical imaging-based diagnosis focuses on X-ray⁷, CT⁸, MRI⁹ or two-dimensional (2D) ultrasound images¹⁰. CAD systems can assist radiologists in distinguishing the benign and malignant nodules in ultrasonic images¹¹. However, most of these systems only work for static images. CAD systems for video tasks not only need massive medical video data that are difficult to obtain but also need to model long-range temporal information, which is difficult to calculate^{12,13}. Although there is an echocardiogram measurement system based on deep neural network¹⁴, there is no available CAD tool that is able to determine the number of patients' nodules (it is important to note that this is different from counting the number of regions of interests in 2D slices), distinguish different nodules, and identify the same nodules in different frames of an ultrasound video for per-nodule analysis or across different videos acquired at different time points for prognosis management purposes.

Re-identification (Re-ID) is an important task in computer vision that searches for real matches of a given query from a large repository containing non-overlapping camera images/videos¹⁵. The Re-ID methods based on deep neural networks are mainly applied to

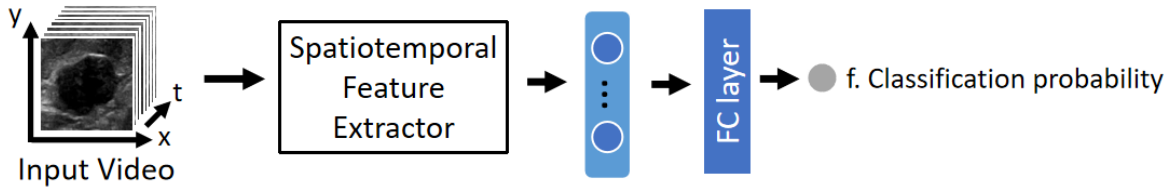
smart city surveillance¹⁶. And it has been applied in CT images¹⁷ but not in ultrasound videos. There are several factors that affect the effectiveness of the Re-ID process, such as the variability of the image foreground and background, low resolution etc¹⁸. For ultrasonic images, the former can be caused by compression deformation of tissue and respiratory cycle during scanning as well as time development of nodules while the latter is an inherent drawback of ultrasonics. Therefore, there is an unmet clinical need to reliably identify and differentiate or in other words re-identify individual nodules in different ultrasound scanning videos to assist radiologists in rapid and accurate clinical diagnosis and long-term follow-up. This work aims to take an initial step in this direction and propose novel automated methods to identify the same nodules present in different ultrasound videos, taking breast ultrasound scans as an example. It shall be noted that compared to the thyroid, which mainly requires scanning in transverse and longitudinal planes¹, breast ultrasound scanning is more flexible and complex⁵, which makes the task of nodule re-identification in the breast more challenging. As far as we know, this is the first time to address the problem and realize nodule re-identification in ultrasound videos through deep learning technology. So far(August 2023), by searching "ultrasound re-identification" on Google, only a bachelor thesis was found, that investigated the fetal ultrasound image re-identification problem using the deep learning method¹⁹. No related work was found by retrieving "ultrasound nodule matching". In contrast, by retrieving "CT nodule re-identification", two paper works^{17,20} were found for CT temporal nodules matching. In terms of the dataset, no available ultrasound re-identification dataset was found after extensively searching open-source data repositories^{21,22,23}.

A unified step in many computer vision tasks (e.g. classification, recognition, clustering) is to map the raw data to an embedding, which is called representation learning(or feature learning). Representation learning can be normally achieved by supervised learning methods, among which classification and verification are two common choices in the area of Re-ID^{24,25,26,27}. A large proportion of Re-ID works are about tracing humans which utilize personal identity as labels to fit a classifier during the training phase and use it as a feature extractor after discarding the last fully connected layers during the inference phase. The verification method is routinely accomplished by a Siamese Neural Network (SNN)²⁸ which was first introduced for the purpose of signature verification. A typical SNN architecture consists of two identical convolution sub-networks, connected by a binary classification head that predicts similarity between two inputs of the sub-networks.

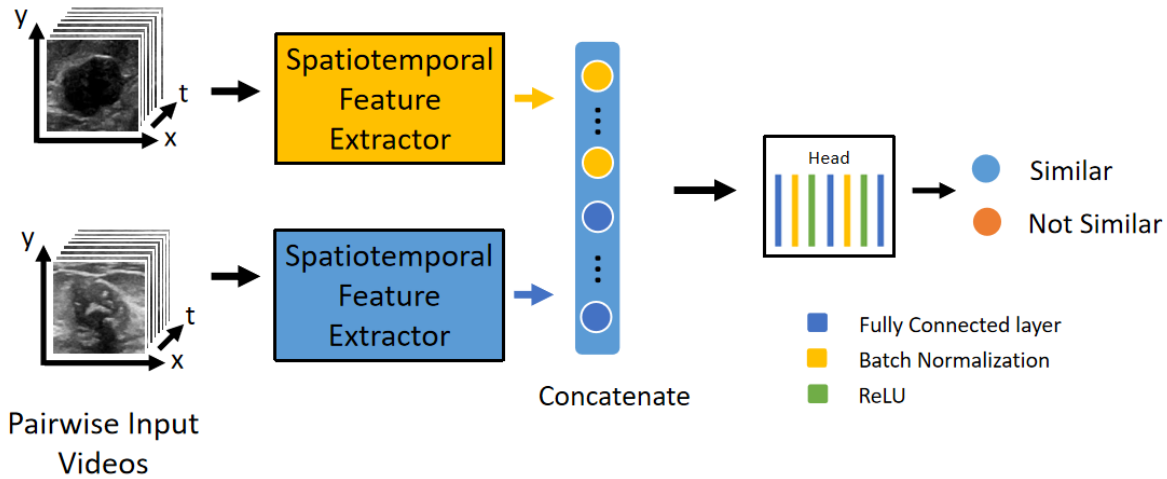
Another topic that is closely related to representation learning is metric learning^{29,30,31}, which tends to learn representation in an implicit way by gathering similar features together and separating dissimilar ones apart through certain distance metrics. Among various metrics, contrastive loss³² and triplet loss²⁹ are the most popular ones. Contrastive loss runs over pairs of samples among which only similar pairs and dissimilar pairs with large enough distances contribute to the last loss (detailed introduction later in the method section) and is widely adapted in self-supervised learning^{33,34}. Instead of taking a pair as input, triplet loss expects a triplet consisting of two matching samples and a non-matching sample and analogously aims to set the negative apart by a distance margin. Most Re-ID algorithms are usually an integration of representation learning and metric learning¹⁸.

Early Re-ID methods mainly tackle the image Re-ID problem. With the emergence of large video Re-ID datasets^{35,36}, more 3D Re-ID architectures are explored^{37,38,39}. Many works focus on properly modeling spatial and temporal information. There are also works that apply optical flow, recurrent neural network, and 3D convolution to perform temporal integration respectively^{37,38}. Recently, unsupervised techniques have been proposed to relieve the heavy workload of data annotation⁴⁰.

Compared to the well-studied person Re-ID problem, there have been very few studies in the medical imaging field. Several commercial CAD systems relying on registration techniques achieved high accuracy in matching lung nodules in CT scans. A 3D SNN based on ResNet-34 architecture was proposed to automatically re-identify pulmonary nodules without image registration¹⁷.⁴¹ employed SNNs to retrieve similar medical images. A bottleneck of deep learning-based medical image analysis is the lack of labeled data, for which contrastive learning is a good workaround. A self-supervised approach was introduced to locate the same anatomical structure across varying images using contrastive learning, which outperforms the supervised method⁴⁰. However, so far as we know, no previous research has investigated the nodule Re-ID problem in ultrasound videos.



(a) Classification model



(b) Verification model

Figure 1: Model structures of classification and verification model

II. METHODS

We compare two common forms of solutions to the nodule matching problem, i.e. classification and verification as introduced in the related work section. Both models share a common framework which consists of an extraction block and a classification head. To compare the performances of the models, we compute the accuracy, sensitivity, specificity, and AUC value. For statistical analysis, we use Delong test to compare the results of the two models, and the p-value below 0.05 is considered statistically significant.

Extraction block. The extraction block containing extractors aim to extract feature representations from input video clips. An extractor maps a point from the input data space \mathbb{R}^D into an embedding space \mathbb{R}^E , where instances belonging to the same nodule have close representations.

$$f = p_{\theta}(x), x \in \mathbb{R}^D, f \in \mathbb{R}^E. \quad (1)$$

The extraction blocks of both models apply a common extractor, which can be the backbone of any 3D- based classification model, as shown in Fig. 1. The only difference is that the verification model takes pair of video clips as input and extracts features from them simultaneously using two extractors sharing the same architecture and weights while the classification has only one extractor. Following the extraction block, a classification head is leveraged for further processing.

Classification head. The extracted features are fed into the classification head to obtain the final class scores. Essentially, both models formulate the Re-ID task as a classification problem. The classification method treats it as a multi-classification problem with a quite large number of categories(702 in our case and can be million in applications like face recognition). Different from some other classification problems with hierarchical categorical structures(fine-grained categories can be aggregated to more general groups and form a tree diagram), our labels present a flat structure that each nodule is a unique category and therefore without overlap between categories. However, ordinary classification is not feasible for such a large-scale classification problem. An alternative is to introduce a triplet loss which is explained in [loss function](#). This loss will force the model to learn the feature representation of the input video clip and enhance the generalization ability. A fully connected layer(FCL) is utilized to classify the feature representation, which is however abandoned in the inference stage, and similarity between two video clips is measured by some distance metric between corresponding representations (e.g. euclidean distance or cosine similarity). The verification method attacks the problem in a straightforward way by training a discriminator to classify representation pairs. As shown in Fig. 1, two feature representations are first concatenated on which a binary classification is conducted by a classification head consisting of multiple FCLs. Similar to the classification model, a contrastive loss is imposed to help with training.

Train and inference pipeline. Despite the obvious difference in the model structures, these two methods actually follow an analogical training pipeline. It's worth noting that for the classification model, we cannot identify unseen nodules, thus it's not feasible to differentiate nodules by predicting their identities. Nevertheless, representations belonging to the same nodule are expected to be close in the feature space and thus a workaround is to compare the feature representations. To this end, the classification head is discarded and only the extractor is employed to extract features from the input video clip. Thereafter we are able to compare two video clips by calculating the cosine similarity between two feature

vectors,

$$S_C(f_1, f_2) = \frac{f_1 \cdot f_2}{\|f_1\| \cdot \|f_2\|}, \quad f_i = p_\theta(x_i), \quad i = 1, 2. \quad (2)$$

where x_i is the input video clip and f_i is the corresponding feature representation. The verification model tackles the problem in a consistent way such that the normalized output of the classification head is naturally a metric for the feature space. Table 1 summarizes the configurations of two models, which will be described in detail in the next sections.

Method	Input	Classification head	Loss	Distance map
CM	Single clip	Single FCL	CE and triplet loss	Cosine distance
VM	Pair of clips	Multiple FCLs	CE and contrastive loss	FCLs

Table 1: Differences between the classification and the verification model. CM=classification model, VM=verification model, CE=cross-entropy.

II.A. model structure

To extract features from the video tracklet, a fragment of video frames that a unique nodule consecutively appears, we utilize the backbone of the R(2+1)D model¹², which consists of spatiotemporal convolution layers that decomposes a 3D convolution into the temporal and spatial parts instead of using a full 3D convolution, as shown in Fig. 2. During training, spatial features are first extracted from the input tensor, and then temporal information is integrated. Like most neural network classification architectural designs, both classification and verification models employ FCL(s) as classifiers. For the classification model, a simple FCL is applied to assign probabilities to classes in the training phase but is abandoned during inference. For the verification model, two feature extractors that have the same structure and share the same weights are used to extract features from a pair of inputs. To further blend the extracted features, a couple of FCLs are exploited: First, two feature embeddings are concatenated. The first two FCLs reduce the feature dimension and the third one computes a similarity score. As shown in Fig 1, a batch norm layer and a relu activation layer are appended between the intermediate FCLs to decrease overfitting and increase nonlinearity respectively.

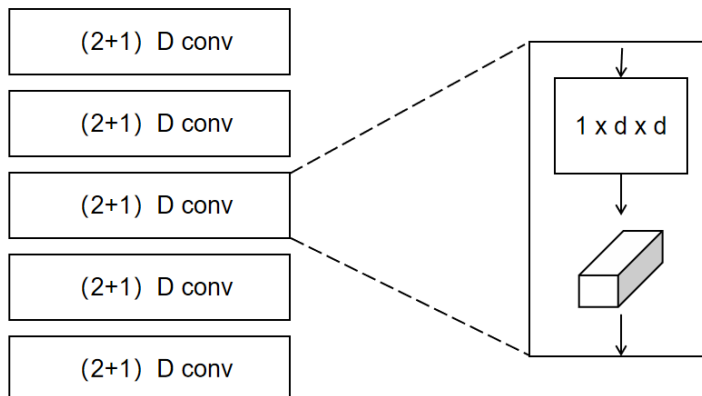


Figure 2: backbone for feature extraction of both classification and verification models
II.B. loss function

The loss function is crucial in the Re-ID problem. An elementary loss for the classification problem is the cross-entropy loss which penalizes predicted probabilities that are far from the ground truth label. In both classification and verification models, we utilize the cross-entropy loss and refer to it as classification loss and verification loss respectively according to their application scenarios. Numerous parameters are discarded due to the withdrawal of the classifier after training in the classification model. To enhance the classification model's ability of feature extraction we use a revised TriHard loss⁴² that mines hard triplets. Let $D(x, y)$ denote the distance metric in the embedding space, and $D_{i,j}$ denote the distance between extracted features of input data x_i and x_j ,

$$D_{i,j} = D(p_{\theta}(x_i), p_{\theta}(x_j)), \quad x_i, x_j \in \mathbb{R}^D. \quad (3)$$

The key idea contains two steps: First collect $P \times K$ samples consisting of P classes, each with K video tracklets, to form a training batch X . Then for each sample a , pick the hardest positive and negative sample to compute the triplet loss:

$$\mathcal{L}_{\text{trip}}(X) = \sum_{i=1}^{\overbrace{P \quad K}^{\text{all anchors}}} \sum_{a=1}^{\overbrace{P \quad K}^{\text{all anchors}}} \max \left[0, m + \overbrace{\max_{p=1 \dots K} D(p_{\theta}(x_a^i), p_{\theta}(x_p^i))}^{\text{hardest positive}} - \overbrace{\min_{\substack{j=1 \dots P \\ n=1 \dots K \\ j \neq i}} D(p_{\theta}(x_a^i), p_{\theta}(x_n^j))}^{\text{hardest negative}} \right], \quad (4)$$

where x_j^i indicates the j -th tracklet of the i -th nodule. This sampling strategy increases the total triplet number that contributes to the loss. Combine with the classification loss

$$\mathcal{L}_{\text{class}}(X) = -\frac{1}{PK} \sum_{k=1}^{PK} \sum_{i=1}^C y_i \log(\text{softmax}(p_\theta(x))_i), \quad (5)$$

we obtain the ultimate loss for a training batch:

$$\mathcal{L}(X) = \mathcal{L}_{\text{class}}(X) + \mathcal{L}_{\text{trip}}(X). \quad (6)$$

For the verification model, we employ the cross-entropy loss and the contrastive loss:

$$\mathcal{L}(X) = \mathcal{L}_{\text{cross}}(X) + \mathcal{L}_{\text{con}}(X), \quad (7)$$

$$\mathcal{L}_{\text{cross}}(X) = \frac{1}{N} \sum_{i=1}^N y_i \log(\text{softmax}(g_\beta(q_\theta(x_i^1, x_i^2))))), \quad (8)$$

$$\mathcal{L}_{\text{con}}(X) = \frac{1}{2N} \sum_{i=1}^N [y_i d_i^2 + (1 - y_i) \max(0, m - d_i)], \quad (9)$$

where $d_i = \|p_\theta(x_i^1) - p_\theta(x_i^2)\|_2$ is the euclidean distance between the extracted features of the input pair and N is the batch size. $y_i = 1$ if the inputs belong to the same nodule and $y_i = 0$ otherwise.

II.C. clustering

Re-ID can be applied to count the number of nodules in a video by grouping individual nodule tracklets. To this end, there is a need for highly accurate clustering algorithm applicable to high dimensional features, while requiring no presumed number of clusters (or nodules) and at the same time suitable for both the classification and verification model we propose. We have evaluated popular methods such as MeanShift⁴³, Density-Based Spatial Clustering of Applications with Noise (DBSCAN)⁴⁴ etc. These methods often make assumptions about the data distribution. For instance, DBSCAN requires the data density to be close. In contrast, our method merely computes and compares pairwise distance without any assumption on the data. After obtaining the embedded features $F = \{f_1, f_2, \dots, f_n\}$ of a video, we first initialize a new cluster, which contains all the categorized features that belong to a unique nodule, with a randomly selected feature \bar{f} from F . Then we compare all the unclassified features with the categorized ones. If a feature in F is close enough to any elements in the cluster, it is included in the cluster and excluded from F . This procedure is repeated until all the features are categorized and we get the final clusters.

Algorithm 1 nodules clustering algorithm

```

Input  $F = \{f_1, f_2, \dots, f_n\}$ , threshold  $\tau$ , distance map  $d(\cdot)$ 
 $clusters = \{\}$ 
while  $|F| > 0$  do
  randomly select  $\tilde{f} \in F$ 
   $cluster = \{\tilde{f}\}$ 
   $F = F \setminus \{\tilde{f}\}$ 
  for each  $f \in F$  do
    if  $\exists \tilde{f} \in cluster$ , such that  $d(\tilde{f} - f) < \tau$  then
       $cluster = cluster \cup \{f\}$ 
    end if
  end for
   $F = F \setminus cluster$ ,  $clusters = clusters \cup cluster$ 
end while
return  $clusters$ 

```

II.D. Dataset

We trained and validated our algorithm on the breast ultrasound dataset. Analysis of breast nodules is important for the diagnosis of breast cancer, which has the highest incidence rate among women. Ultrasound examination is an efficient method for breast screening, during which inspections are conducted repeatedly and numerous video clips containing nodules are generated. These video clips may consist of single or multiple nodules and thus are proper to validate our algorithm.

	Patient	Nodule	Tracklet
Training	623	702	2683
Validation	76	85	317
Test	88	98	409

Table 2: Datasets statistics.

Data acquisition. The video dataset was collected from the Second Affiliated Hospital of Nanchang University. As summarized in Table 2, 787 patients containing 885 nodules and 3409 tracklets were included in total. The length of tracklets ranges from 1 to 2122. The distribution is shown in Fig. 3. All tracklets were first grouped by the patient identity and then randomly split into training, validation and test sets with a rough ratio of 8:1:1. In this dataset, several nodules may be present in a single video and the same nodule might appear multiple times as well (one video corresponds to one patient). Videos were annotated manually by expert radiologists at pixel-level. A single video can be divided into

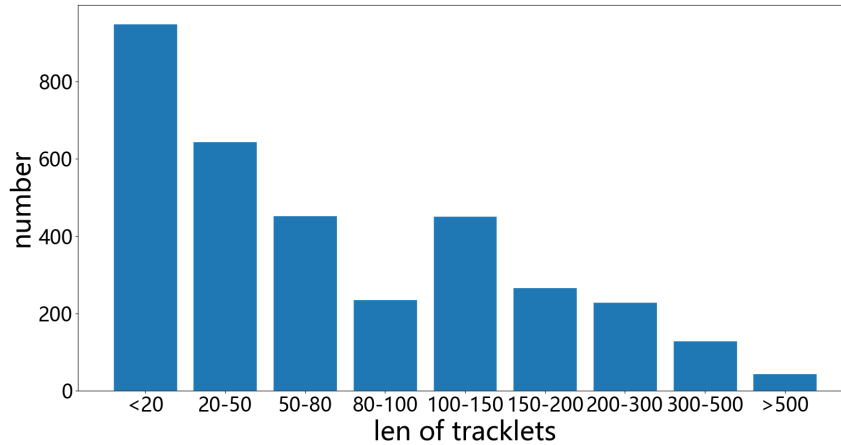


Figure 3: Distribution of the length of tracklets in the overall dataset. several tracklets. However, it is important to note that various tracklets may overlap in the same frame where multiple nodules can be present simultaneously. The annotation process followed the guidelines below:

- The starting and the ending frame of a tracklet must be annotated,
- Key frames with drastic change of nodule morphology must be annotated.

Preprocessing. Following the common processing pipeline of person re-identification benchmark, we extracted the patches containing the target object from the video frames. Since only the key frames are annotated, the union of adjacent key frames was taken as the annotation for the intermediate frames. After cropping the ROI from the original video frames, all patches were resized to 256×128 , as illustrated in Fig 4.

II.E. Implementation details

To generate the paired data for the training of the verification method, we randomly selected a positive tracklet (of the same nodule) and a negative tracklet (of a different nodule) from the same patient for every tracklet. For the validation and test set, we paired each tracklet with all the other tracklets from the same patient and evaluated our models on these pairs. We trained both models on the train set and took the one that achieved the best accuracy on the validation set for the final evaluation on the test set. The Adam with initial learning rate 1×10^{-4} and weight decay 5×10^{-4} was adopted for training. As aforementioned, in the

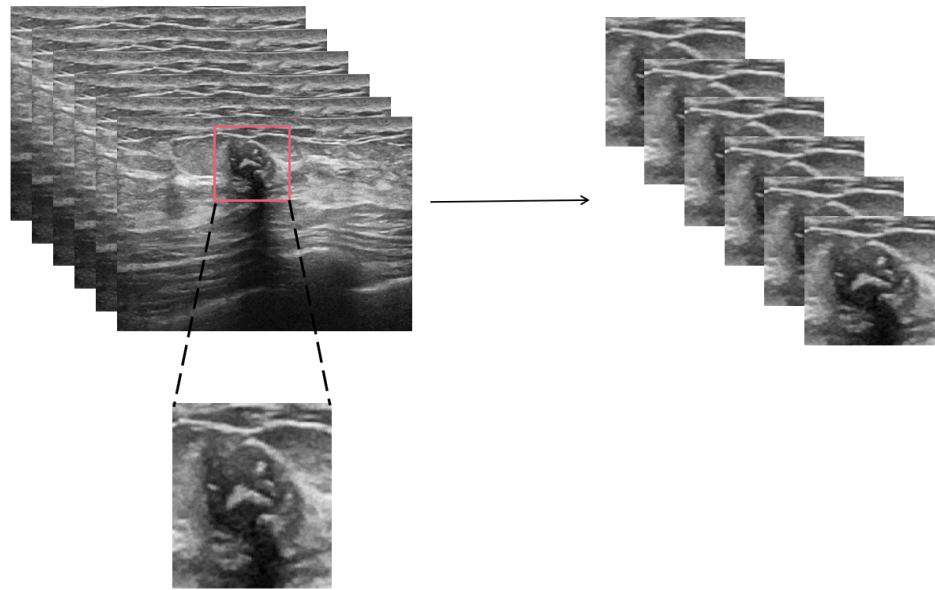


Figure 4: Preprocessing of the ultrasound Re-ID dataset. Patches containing the target objects were extracted from the original frames.

training stage, we treated the classification method as a normal classification problem while in the valid and test stages, the fully connected layer was discarded and the cosine distance was utilized to measure the similarity between the extracted features. All experiments were conducted using PyTorch 1.7.0 on four Tesla P40 GPUs.

III. RESULTS

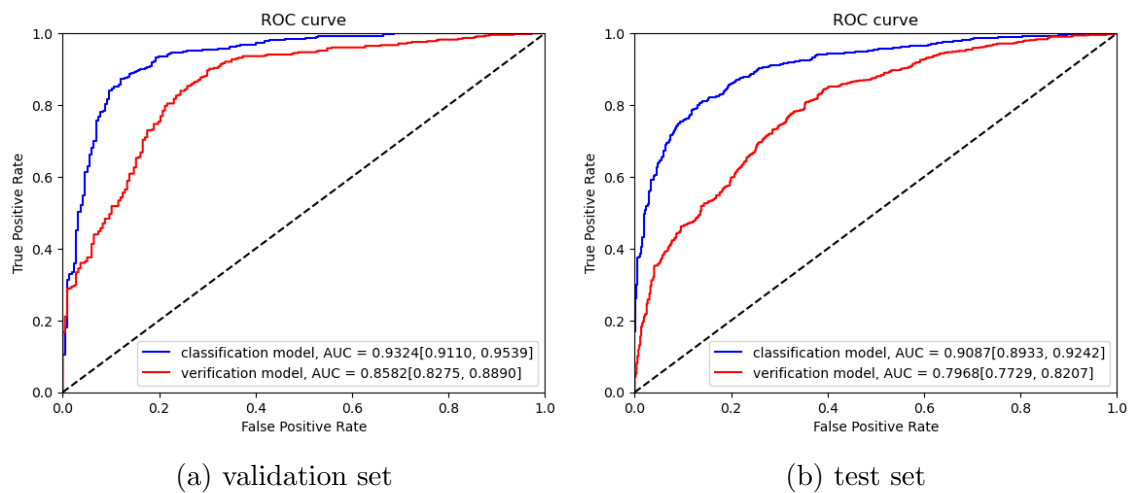


Figure 5: ROC curves for the two models on validation and test sets.

The performances of the two methods are shown in Fig. 5 and Table 3. We compared

the efficacy of the two methods using the ROC curves and the associated Area Under the Curve (AUC) values. Fig. 5a and Fig. 5b show the ROC curve of validation and test set respectively. The classification model outperformed the verification model on both sets, with a higher AUC value of 0.9324 in the validation set and an AUC value of 0.9087 in the test set. The verification model achieved AUC values of 0.8582 and 0.7968 respectively. Table 3 summarizes the accuracy, sensitivity, and specificity of both methods in different phases. Compared with the verification model, the classification model has better performance in all three metrics. The verification model achieves higher sensitivity than specificity by a large margin(over 10% in the test set), which suggests it struggles to differentiate dissimilar samples.

	ACC(95%CI)	SE(95%CI)	SP(95%CI)	AUC(95%CI)
Validation set				
Classification model	87.84(85.54-89.89)	89.01(86.30-91.26)	84.88(79.79-88.95)	93.24(91.10-95.39)
Verification model	79.74(76.98-82.30)	81.98(78.78-84.82)	74.03(68.15-79.20)	85.82(82.75-88.90)
Test set				
Classification model	84.78(82.97-86.46)	86.78(84.60-88.71)	80.97(77.48-84.05)	90.87(89.33-92.42)
Verification model	74.69(72.53-76.75)	79.12(76.57-81.47)	66.26(62.22-70.09)	79.68(77.29-82.07)

Table 3: Performance measures for the two models. ACC=Accuracy, SE=Sensitivity, SP=Specificity, 95%CI=Confidence interval of 95%. Comparisons of two models on both validation and test set were performed by Delong test and p-value < 0.001 in both cases.

Comparison of different clustering algorithms

We compared our method with several commonly used clustering algorithms implemented in the sklearn library in the test set. To this end, feature representations from video tracklets were extracted using the classification model, which achieved better accuracy in the previous experiment. We first conducted a clustering algorithm on each video and accumulated all results to calculate the evaluation metrics. The accuracy performances were evaluated in pairwise recall, pairwise precision and the F-score, which is the harmonic mean of recall and precision. We also measured the time all algorithms cost, which is important in real applications. For all algorithms, we tuned the hyperparameters and took the best results. As summarized in Table 4, DBSCAN tends to group dissimilar features into the same cluster such that it reaches a recall of 1 and a low precision of 71.74. In contrast, MeanShift and AffinityPropagation obtain high precision but suffer from very low recall. Our clustering algorithm outperforms all methods in F-score, which indicates its effectiveness. Specifically, it obtains the highest recall among the four algorithms and achieves comparable precision.

In terms of efficiency, all algorithms are able to process hundreds of samples in real time except DBSCAN and our clustering algorithm consumes the least time. To get an intuitive

Methods	Precision	Recall	F-score	Time(s)
DBSCAN ⁴⁴	71.74	100.00	83.55	3.09
MeanShift ⁴³	93.56	18.42	30.78	0.003
AffinityPropagation ⁴⁵	97.35	56.70	71.67	0.005
Ours	85.96	90.69	88.26	< 0.001

Table 4: Comparison of different clustering methods.

impression of these algorithms, we visualize a typical clustering result. As can be seen from Fig. 6, DBSCAN clusters all the tracklets into one category. On the contrary, Meanshift divides all the tracklets into different clusters. Both algorithms fail to cluster totally. Relative satisfactory clustering results are achieved by AffinityPropagation and our algorithm. Unfortunately, AffinityPropagation mistakenly clusters three circles into a separate group while our algorithm improperly groups a star with circles.

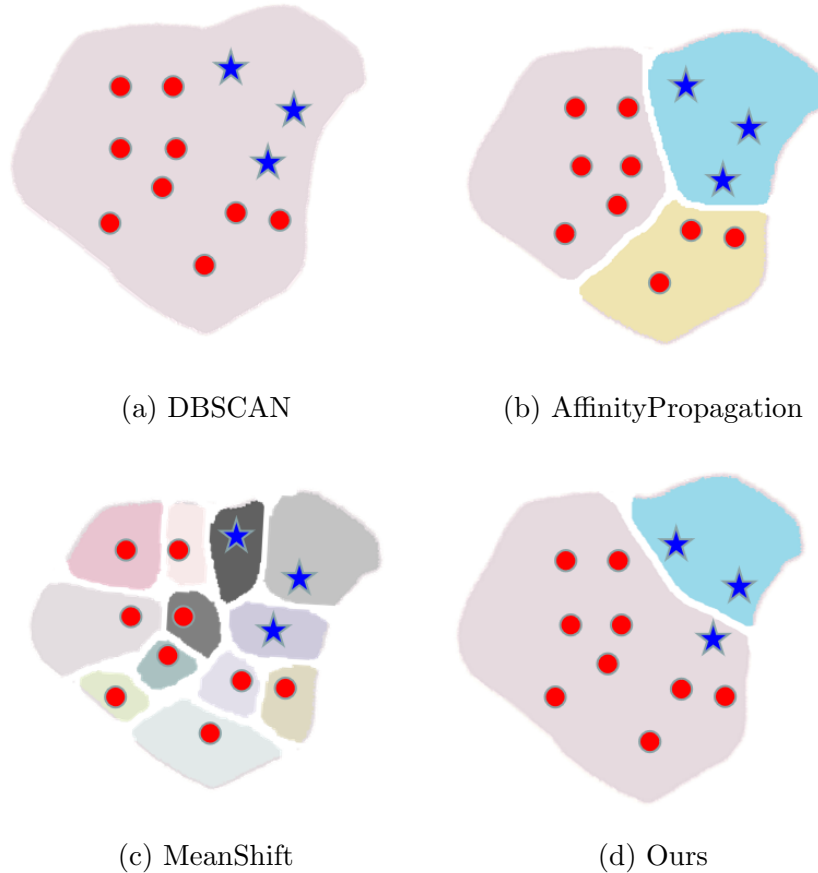


Figure 6: Visualization of typical results obtained by four clustering algorithms. Feature points from different nodules are marked with different symbols. The results of clustering are indicated by different color patches

IV. DISCUSSION

It is helpful to quickly and accurately re-identify different ultrasonic scans. For instance, the diagnosis of benign and malignant nodules needs careful inspections in multiple cross-sectional views of a nodule to recognize key diagnostic features. In practice, the sonographer needs to keep scanning to identify representative frames of the nodule. Since multiple nodules are quite common, sonographers usually differentiate nodules by comparing surrounding anatomical morphology between frames, which is cumbersome and time-consuming. With the Re-ID and clustering algorithms, we can easily collect numerous representative frames and automatically group them by nodules.

As far as we know, there is no commercial software or academic study on the re-identification problem of ultrasonic videos yet. To accomplish this task, we collected hun-

dreds of ultrasound videos and made an ultrasonic ReID dataset. Based on this dataset, which covers more than 800 cases of breast nodules, we built a nodule re-identification system. In particular, two common re-identification algorithms were compared. The classification model treats the Re-ID as a generic multi-classification problem such that each nodule is a unique class and the verification model differentiates a pair of video clips directly. In terms of the loss function, the classification method leverages multi-class cross-entropy and TriHard loss while the verification method employs binary cross-entropy and contrastive loss. To evaluate the performances of the two methods, we calculate the pairwise accuracy, sensitivity and specificity. Our experimental results(Fig. 5 and Table 3) show that the classification model outperforms the verification model by a large margin(around 8% and 10% in accuracy in the validation and test set respectively) and is capable to differentiate ultrasound videos. Using the Re-ID algorithm, we can count the number of nodules by applying a clustering algorithm on the extracted feature vectors. After trying several popular clustering algorithms without satisfactory results, we proposed a novel algorithm that achieves better results while costing the least time(Table 4 and Fig6). To be specific, in terms of efficiency, our algorithm takes less than 0.001s while MeanShift and AffinityPropagation take 0.003s and 0.005s respectively. The widely used DBSCAN takes more than 3s. Our algorithm also obtains the highest F-score of 88.26, surpassing the other three methods. Actually, all these methods fail to cluster the features in our case. DBSCAN groups each feature into a cluster and thus obtains a recall of 100 and a precision of 71.74. MeanShift and AffinityPropagation tend to group dissimilar features in the same group such that they obtain high precision(93.56 and 97.35 respectively) and extremely low recall(18.42 and 56.70 respectively). Although our algorithm is the only feasible method, there is still room for improvement in accuracy. The feature clustering problem in our case faces a difficulty called curse of dimensionality such that the most commonly used clustering algorithms fail to work. The key issue is that as the dimensionality increases, the distribution of the data points becomes sparse. Research on clustering on high-dimensional features is active in recent years and several methods based on Graph Convolutional Networks(GCN) were proposed in^{46,47}.

There are several limitations of our study. First, the dataset is not sufficiently large compared to MARS³⁵ dataset in person re-identification, which contains 1,261 IDs and around 20,000 tracklets. It is worthy of further investigation into whether a larger dataset will enhance the model. Furthermore, it is meaningful to compare current and follow-up

nodules to evaluate the development of potential lesions. Due to the lack of data, we are not able to verify the algorithm’s ability to discriminate such nodules.¹⁷ gives a good example of such an investigation. It’s worth noting that re-identification technology also plays an important role in some other medical applications. For example,⁴⁸ uses it for nodule tracking.

V. CONCLUSION

In this paper, we address the problem of automatic differentiation ultrasound videos using a CNN-based feature extractor and efficient clustering post-processing. For the extractor, we implemented two popular Re-ID models and compared their pairwise accuracy. The best result reached accuracies of 0.88 and 0.85 on the validation and test set respectively, showing the capability of the algorithm to effectively differentiate ultrasound videos. For the clustering post-processing, we proposed a novel algorithm that outperforms the commonly used clustering algorithms both in accuracy and efficiency. We regard this work as a preliminary study for two reasons: First, clinicians may have interest in the development of certain nodules and the algorithm’s capability to distinguish current and follow-up ultrasound scans remains to be confirmed. Second, compared to the high accuracy achieved in the area of person re-identification, our framework still needs improvement to better meet the demands of clinical practice. We will focus on these limitations for further investigation.

Acknowledgements

This work was supported in part by the National Natural Science Foundation of China (Grant Nos. 12126607, 91859201) and the Key Research and Development Project from Science and Technology Department of Jiangxi Province (Grant Nos. 20202BBGL73032, 20223BBG71005).

Conflict of interest

No conflicts of interest.

References

- ¹ B. R. Haugen, E. K. Alexander, K. C. Bible, et al., 2015 American Thyroid Association Management Guidelines for Adult Patients with Thyroid Nodules and Differentiated Thyroid Cancer: The American Thyroid Association Guidelines Task Force on Thyroid Nodules and Differentiated Thyroid Cancer, *Thyroid : official journal of the American Thyroid Association* **26**, 1–133 (2016), [Online; accessed 2022-12-13].
- ² A. L. Siu and U. P. S. T. Force, Screening for Breast Cancer: U.S. Preventive Services Task Force Recommendation Statement, *Annals of internal medicine* **164**, 279–96 (2016), [Online; accessed 2022-12-13].
- ³ J. K. Heimbach, L. M. Kulik, R. S. Finn, et al., AASLD guidelines for the treatment of hepatocellular carcinoma, *Hepatology* **67**, 358–380 (2018).
- ⁴ J. M. Weigert and S. Steenbergen, The Connecticut Experiment: The Role of Ultrasound in the Screening of Women With Dense Breasts, *The Breast Journal* **18** (2012).
- ⁵ C. M. Vogel-Minea, W. Bader, J.-U. Blohmer, et al., Best Practice Guideline - DEGUM Recommendations on Breast Ultrasound, *Ultraschall in der Medizin (Stuttgart, Germany : 1980)* (2023).
- ⁶ M. Abadi, A. Chu, I. Goodfellow, et al., Deep Learning with Differential Privacy, in *Proceedings of the 2016 ACM SIGSAC Conference on Computer and Communications Security, CCS '16*, page 308–318, New York, NY, USA, 2016, Association for Computing Machinery.
- ⁷ D. S. Kermany, M. Goldbaum, W. Cai, et al., Identifying Medical Diagnoses and Treatable Diseases by Image-Based Deep Learning, *Cell* **172**, 1122–1131.e9 (2018), [Online; accessed 2022-12-13].
- ⁸ F. Shi, J. Wang, J. Shi, et al., Review of Artificial Intelligence Techniques in Imaging Data Acquisition, Segmentation, and Diagnosis for COVID-19, *IEEE reviews in biomedical engineering* **14**, 4–15 (2021), [Online; accessed 2022-12-13].
- ⁹ W. L. Bi, A. Hosny, M. B. Schabath, et al., Artificial intelligence in cancer imaging: Clinical challenges and applications, *CA: a cancer journal for clinicians* **69**, 127–157 (2019), [Online; accessed 2022-12-13].

- ¹⁰ T. Wu, L. R. Sultan, J. Tian, et al., Machine learning for diagnostic ultrasound of triple-negative breast cancer, *Breast cancer research and treatment* **173**, 365–373 (2019), [Online; accessed 2022-12-13].
- ¹¹ A. Pfob, C. Sidey-Gibbons, R. G. Barr, et al., The importance of multi-modal imaging and clinical information for humans and AI-based algorithms to classify breast masses (INSPIRED 003): an international, multicenter analysis, *European radiology* **32**, 4101–4115 (2022), [Online; accessed 2022-12-13].
- ¹² D. Tran, H. Wang, L. Torresani, et al., A Closer Look at Spatiotemporal Convolutions for Action Recognition, *CoRR* **abs/1711.11248** (2017).
- ¹³ Y. Zhu, X. Li, C. Liu, et al., A Comprehensive Study of Deep Video Action Recognition, *ArXiv* **abs/2012.06567** (2020).
- ¹⁴ D. Ouyang, B. He, A. Ghorbani, et al., Video-based AI for beat-to-beat assessment of cardiac function, *Nature* **580**, 252–256 (2020).
- ¹⁵ S. U. Khan, T. Hussain, A. Ullah, et al., Deep-ReID: deep features and autoencoder assisted image patching strategy for person re-identification in smart cities surveillance, *Multimedia Tools and Applications* (2021).
- ¹⁶ A. Ullah, K. Muhammad, T. Hussain, et al., Conflux LSTMs Network: A Novel Approach for Multi-View Action Recognition, *Neurocomputing* **435**, 321–329 (2021).
- ¹⁷ X. Rafael-Palou, A. Aubanell, I. Bonavita, et al., Re-Identification and growth detection of pulmonary nodules without image registration using 3D siamese neural networks, *Medical Image Analysis* **67**, 101823 (2021).
- ¹⁸ M. Ye, J. Shen, G. Lin, et al., Deep Learning for Person Re-Identification: A Survey and Outlook, *IEEE Transactions on Pattern Analysis and Machine Intelligence* **44**, 2872–2893 (2022).
- ¹⁹ unknown, Fetal Re-Identification: Deep Learning on Pregnancy Ultrasound Images, (2022).
-

- ²⁰ C. Tao, D. S. Gierada, F. Zhu, et al., Automated matching of pulmonary nodules: evaluation in serial screening chest CT, *American Journal of Roentgenology* **192**, 624–628 (2009).
- ²¹ medical-datasets, <https://github.com/adalca/medical-datasets> .
- ²² paperswithcode, <https://paperswithcode.com/datasets> .
- ²³ awesome-reid-dataset, <https://github.com/NEU-Gou/awesome-reid-dataset> .
- ²⁴ R. R. Varior, M. Haloi, and G. Wang, Gated Siamese Convolutional Neural Network Architecture for Human Re-Identification, *CoRR* **abs/1607.08378** (2016).
- ²⁵ Y. Lin, L. Zheng, Z. Zheng, et al., Improving Person Re-identification by Attribute and Identity Learning, *CoRR* **abs/1703.07220** (2017).
- ²⁶ T. Matsukawa and E. Suzuki, Person re-identification using CNN features learned from combination of attributes, in *2016 23rd International Conference on Pattern Recognition (ICPR)*, pages 2428–2433, 2016.
- ²⁷ L. Zheng, Y. Yang, and A. Hauptmann, Person Re-identification: Past, Present and Future, *ArXiv* **abs/1610.02984** (2016).
- ²⁸ J. Bromley, I. Guyon, Y. LeCun, et al., Signature Verification using a "Siamese" Time Delay Neural Network, in *Advances in Neural Information Processing Systems*, edited by J. Cowan, G. Tesauro, and J. Alspector, volume 6, Morgan-Kaufmann, 1993.
- ²⁹ F. Schroff, D. Kalenichenko, and J. Philbin, FaceNet: A unified embedding for face recognition and clustering, in *2015 IEEE Conference on Computer Vision and Pattern Recognition (CVPR)*, pages 815–823, 2015.
- ³⁰ A. Hermans, L. Beyer, and B. Leibe, In Defense of the Triplet Loss for Person Re-Identification, *CoRR* **abs/1703.07737** (2017).
- ³¹ Q. Xiao, H. Luo, and C. Zhang, Margin Sample Mining Loss: A Deep Learning Based Method for Person Re-identification, *CoRR* **abs/1710.00478** (2017).

-
- ³² R. Hadsell, S. Chopra, and Y. LeCun, Dimensionality Reduction by Learning an Invariant Mapping, in *2006 IEEE Computer Society Conference on Computer Vision and Pattern Recognition (CVPR'06)*, volume 2, pages 1735–1742, 2006.
- ³³ K. He, H. Fan, Y. Wu, et al., Momentum Contrast for Unsupervised Visual Representation Learning, in *2020 IEEE/CVF Conference on Computer Vision and Pattern Recognition (CVPR)*, pages 9726–9735, 2020.
- ³⁴ T. Chen, S. Kornblith, M. Norouzi, et al., A Simple Framework for Contrastive Learning of Visual Representations, CoRR **abs/2002.05709** (2020).
- ³⁵ L. Zheng, Z. Bie, Y. Sun, et al., MARS: A Video Benchmark for Large-Scale Person Re-Identification, in *Computer Vision – ECCV 2016*, edited by B. Leibe, J. Matas, N. Sebe, et al., pages 868–884, Cham, 2016, Springer International Publishing.
- ³⁶ L. Zheng, L. Shen, L. Tian, et al., Scalable Person Re-identification: A Benchmark, in *2015 IEEE International Conference on Computer Vision (ICCV)*, pages 1116–1124, 2015.
- ³⁷ S. Xu, Y. Cheng, K. Gu, et al., Jointly Attentive Spatial-Temporal Pooling Networks for Video-based Person Re-Identification, CoRR **abs/1708.02286** (2017).
- ³⁸ B. Zhou, A. Khosla, À. Lapedriza, et al., Learning Deep Features for Discriminative Localization, CoRR **abs/1512.04150** (2015).
- ³⁹ R. Hou, H. Chang, B. Ma, et al., BiCnet-TKS: Learning Efficient Spatial-Temporal Representation for Video Person Re-Identification, CoRR **abs/2104.14783** (2021).
- ⁴⁰ K. Yan, J. Cai, D. Jin, et al., SAM: Self-Supervised Learning of Pixel-Wise Anatomical Embeddings in Radiological Images, *IEEE Transactions on Medical Imaging* **41**, 2658–2669 (2022).
- ⁴¹ Y. Cai, Y. Li, C. Qiu, et al., Medical Image Retrieval Based on Convolutional Neural Network and Supervised Hashing, *IEEE Access* **7**, 51877–51885 (2019).
- ⁴² A. Hermans, L. Beyer, and B. Leibe, In Defense of the Triplet Loss for Person Re-Identification, CoRR **abs/1703.07737** (2017).
-

-
- ⁴³ Y. Cheng, Mean shift, mode seeking, and clustering, *IEEE Transactions on Pattern Analysis and Machine Intelligence* **17**, 790–799 (1995).
- ⁴⁴ M. Ester, H. P. Kriegel, J. Sander, et al., A density-based algorithm for discovering clusters in large spatial databases with noise, (1996).
- ⁴⁵ D. Dueck and B. J. Frey, Non-metric affinity propagation for unsupervised image categorization, in *2007 IEEE 11th International Conference on Computer Vision*, pages 1–8, 2007.
- ⁴⁶ Z. Wang, L. Zheng, Y. Li, et al., Linkage Based Face Clustering via Graph Convolution Network, *CoRR* **abs/1903.11306** (2019).
- ⁴⁷ L. Yang, X. Zhan, D. Chen, et al., Learning to Cluster Faces on an Affinity Graph, *CoRR* **abs/1904.02749** (2019).
- ⁴⁸ X. Wu, G. Tan, N. Zhu, et al., CacheTrack-YOLO: Real-Time Detection and Tracking for Thyroid Nodules and Surrounding Tissues in Ultrasound Videos, *IEEE journal of biomedical and health informatics* **25**, 3812–3823 (2021), [Online; accessed 2022-12-13].